Composites Part B 223 (2021) 109096

Contents lists available at ScienceDirect

Composites Part B

journal homepage: www.elsevier.com/locate/compositesb

Combining ultrasound directed self-assembly and stereolithography to fabricate engineered polymer matrix composite materials with anisotropic electrical conductivity

K. Niendorf, B. Raeymaekers *

Department of Mechanical Engineering, University of Utah, Salt Lake City, UT, 84112, USA

ARTICLE INFO

Keywords:
Ultrasound directed self-assembly
Conductive composites
Polymer matrix
Composites
Additive manufacturing

ABSTRACT

Engineered polymer matrix composite materials with designer electrical properties are important for a myriad of engineering applications including flexible electronics, electromagnetic shielding, and materials with embedded electrical wiring. However, existing fabrication methods are limited by material choice and dimensional scalability. We use the acoustic radiation force associated with a standing ultrasound wave field to spatially arrange and align electrically conductive microfibers dispersed in a photopolymer matrix in user-specified orientations and use stereolithography to solidify the material. We relate the electrical conductivity of the material specimens to the fabrication process parameters, including ultrasound transducer power, microfiber alignment, and microfiber weight fraction. Logistic regression analysis demonstrates that the probability that a composite material specimen is electrically conductive increases with increasing microfiber weight fraction and microfiber alignment because these parameters drive the formation of a long-range percolated network of electrically conductive microfibers. We determine that the electrical conductivity of conductive specimens ranges between 31 – 793 S/m and that the fabrication process parameters are critical in predicting whether a composite material specimen is electrically conductive or insulating. Relating the composite material fabrication process parameters to the resulting electrical conductivity is a crucial step towards fabricating polymer matrix composite materials with designer electrical properties for use in engineering applications. The combined ultrasound DSA and SLA fabrication process works independent of fiber and matrix material properties and facilitates dimensional scalability due to low attenuation of ultrasound waves in viscous media.

1. Introduction

Polymer matrix composite materials consist of a polymer matrix and one or more continuous or discontinuous filler materials [1]. Continuous filler material (e.g., fiber tow) typically spans the entire length of the composite material specimen, aligns under mechanical tension during the fabrication process, and serves as mechanical reinforcement to the polymer matrix [2]. Discontinuous filler material may consist of micro- or nanosized particles such as microfibers [3], microrods [4], nanofibers [5], carbon nanotubes (CNTs) [6], or powders consisting of spherical particles [7], to name a few. They either randomly disperse [8] or align in a specified pattern in the polymer matrix [9]. Changing the material properties, weight fraction, and alignment of the discontinuous filler material in the polymer matrix affects the bulk properties of the polymer matrix composite material and how it interacts with an external field (e.g., electric, magnetic, force fields). Thus, these materials can be engineered to display a variety of properties, including designer thermal [10], mechanical [11], or electrical [12] properties. In this paper, we specifically focus on electrical conductivity or, correspondingly, electrical resistance. For instance, aligning electrically conductive filler material in the composite material matrix can function as embedded electrical wiring [13], which is useful to a myriad of engineering applications, including flexible electronics [14], chemical or biological sensors [15], and stretchable strain sensors [16].

We determine the electrical conductivity of a polymer matrix composite material from an electrical resistance measurement, which depends on the electrical properties of the matrix and filler materials [17], and the concentration [18], size [19], and alignment [12] of the filler material within the matrix material. Several methods exist to quantify the electrical resistance of polymer matrix composite materials with

* Corresponding author.
E-mail address: bart.raeymaekers@utah.edu (B. Raeymaekers).

https://doi.org/10.1016/j.compositesb.2021.109096
Received 6 April 2021; Received in revised form 4 June 2021; Accepted 20 June 2021
Available online 24 June 2021

discontinuous filler material. A DC electrometer allows precision high-resistance measurements, but typically only above 10^3 Ohm, thus rendering it unsuitable for electrical conductors [20]. An impedance analyzer measures impedance as a function of frequency, and is typically used to measure AC electrical conductivity [21]. A parameter analyzer measures the DC current as a function of voltage magnitude (max. 10V), which makes it suitable for conductors and semiconductors [12]. Finally, using a high-quality multimeter to measure DC resistance is straightforward and accurate for conductors and semiconductors [22].

Fabricating polymer matrix composite materials with designer electrical properties or embedded electrical wiring requires creating percolated networks of aligned filler material that enable electrical current between different locations in the material. The percolation threshold is defined as the minimum weight fraction of discontinuous filler material that forms long-range connectivity in the material specimen [23]. (Partially) aligning uniformly distributed discontinuous filler material reduces the percolation threshold compared to random or isotropic alignment [24]. Spatially arranging and aligning discontinuous filler material increases the local filler material density and, thus, the probability that individual filler material particles make contact, which decreases the percolation threshold [5], increases electrical conductivity in the alignment direction [25], and decreases electrical conductivity transverse to the alignment direction [26], compared to composite material specimens with randomly oriented (electrically conductive) discontinuous filler material.

Fabricating polymer matrix composite materials with aligned discontinuous filler material requires combining a technique to form the macroscale material specimen geometry with a method to spatially arrange and align filler material within the polymer matrix [27]. Conventional fabrication methods, such as mold casting [28], typically inject a mixture of liquid polymer matrix and filler material into a hollow cavity. Alternatively, additive manufacturing (AM) methods such as stereolithography (SLA), fused filament fabrication (FFF) or fused deposition modeling (FDM), and direct ink writing (DIW) enable the formation of complex free-form geometries in a layer-by-layer fashion without the need for a mold [29]. Our group recently published a comprehensive review on this topic [27].

Several methods exist to spatially arrange and align discontinuous filler material within a polymer matrix material. Researchers have demonstrated that filler material can orient in the direction of an electric [30] or magnetic [31] field, or a combination of both [32]. However, this requires an electrically conductive or ferromagnetic filler material (or coating) and a large external field strength (on the order of 20 kV/m [33] and 8000 mT [34], respectively), which limits dimensional scalability. Khan et al. used a DC electric field within a mold to align multi-walled CNTs (MWCNTs) in epoxy and showed increased electrical conductivity in the alignment direction compared to specimens with randomly oriented MWCNTs [35]. They also documented that electrical conductivity increased with increasing filler material weight fraction. Oliva-Avilés et al. showed anisotropic electrical conductivity in polymer matrix composite materials with CNT filler material that was aligned using an AC and DC electric field, and also documented that electrical conductivity increased with increasing CNT weight fraction [25]. Ma et al. used a magnetic field to align CNTs in epoxy and measured that the electrical conductivity was higher in the direction parallel, as opposed to perpendicular, to the aligned CNTs and also increased with increasing CNT weight fraction [36].

Shear force fields, created by viscous flow of the matrix material with dispersed filler material, typically align filler material in the direction of shear but cannot manipulate spatial arrangement, which limits control over the local filler material density and, thus, the electrical properties of the resulting composite material. Postiglione et al. used DIW in combination with a shear force field, and a mixture of polylactic acid (PLA) and electrically conductive MWCNTs, to 3D print electrically conductive polymer matrix composite materials with aligned MWCNTs [37]. They reported that electrical conductivity increased with increasing MWCNT weight fraction and identified the minimum MWCNT weight fraction required for long-range electrical conductivity.

Ultrasound directed self-assembly (DSA) relies on the acoustic radiation force associated with a standing ultrasound wave field to spatially arrange [38] and orient [39] filler material, independent of material properties or shape [40]. Furthermore, standing ultrasound wave fields display low attenuation in low-viscosity fluids [41], which enhances dimensional scalability compared to other external fields. Melchert et al. fabricated flexible polymer matrix composite materials with ultrasonically aligned carbon and silver-coated glass microfibers, and demonstrated anisotropic electrical conductivity compared to specimens with randomly oriented microfibers [42]. Yunus et al. used a standing ultrasound wave field to align several types of filler material, including copper and magnetite nanoparticles and carbon nanofibers in photocurable polymer [7]. They measured that the electrical conductivity of the resulting composite material increased with increasing filler material weight fraction and depended on the electrical conductivity of the filler material. Greenhall and Raeymaekers used SLA and a standing ultrasound wave field to 3D print photocurable polymer matrix composite materials with aligned nickel-coated carbon microfibers and measured electrical resistance on the order of 10^6 times larger in the direction perpendicular compared to parallel to the microfiber alignment [13].

Table 1 summarizes the literature on fabricating electrically conductive polymer matrix composites materials with discontinuous filler material aligned by means of an external electric, magnetic, shear force, or ultrasound wave field.

The literature documents several methods of fabricating polymer matrix composite materials with percolated networks of electrically conductive microfibers. However, to fabricate polymer matrix composite materials with designer electrical conductivity, one must relate the alignment and orientation of the filler material and its corresponding electrical conductivity or resistance, to the fabrication process parameters. This paper specifically focuses on the combination of SLA and ultrasound DSA because ultrasound functions independent of the filler and matrix material properties and SLA allows selectively curing photopolymer to fixate the filler material in place, without the need for a mold. Thus, this technique offers materials flexibility and dimensional scalability.

The objective of this paper is to characterize the electrical conductivity of polymer matrix composite material specimens as a function of the ultrasound DSA fabrication process parameters, including ultrasound transducer power, microfiber alignment, and microfiber weight fraction. We use multivariate logistic regression analysis to derive a best-fit model that relates whether a polymer matrix composite material specimen conducts electricity to its fabrication process parameters. Additionally, we attempt to relate the electrical conductivity of electrically conductive material specimens to the fabrication process parameters. We present the results in non-dimensional fashion to render them independent of our specific experiment. These results have importance to devising a fabrication process based on standing ultrasound waves and additive manufacturing, which enables implementing polymer matrix composite materials with designer electrical properties for specific engineering applications.

2. Methods

2.1. Fabricating electrically conductive composite material specimens

Fig. 1 schematically shows the experimental apparatus, previously developed by our research group to integrate ultrasound DSA and SLA [13], which we use to fabricate engineered composite material specimens that contain parallel lines of aligned, electrically conductive silver-coated glass microfibers (weight fraction $1.0 \leq w_f \leq 4.0\%$ - measured when mixing the microfibers with the matrix, average diameter 15 μm, average length 130 μm, density 1000 kg/m^3, Potters

Table 1
Overview of external field-based alignment methods of discontinuous filler material in electrically conductive polymer composite materials, identifying specific references, and showing compatible polymer matrices, filler materials, filler material weight fraction w_f, filler material alignment quantification methods, and reported electrical conductivity range. We use the following abbreviations: Polyvinylidene fluoride (PVDF), polysulfone (DPSF), polylactic acid (PLA), carbon nanofibers (CNFs), graphene nanoplatelets (GNPs).

	Electric field	Magnetic field	Shear force field	Ultrasound wave field
Polymer matrix material	• Epoxy [5,22,35,43,44] • PVDF [12] • DPSF [25]	• Epoxy [26,36,44]	• PLA [37]	• Photopolymer [7,13,42,45]
Filler material	• CNTs [12,25,44] • CNFs [5,22,43] • GNPs [5] • MWCNTs [35]	• CNTs [36,44] • GNPs [26]	• MWCNTs [37]	• Ni-coated microfibers [13,45] • Ag-coated microfibers [42] • Carbon microfibers [42] • Magnetite and copper nanoparticles [7] • CNFs [7]
Filler material w_f [%]	0.05 [35] – 3.0 [44]	0.5–5.0 [36]	0.5–10.0 [37]	0.5–9.0 [7]
Filler material alignment quantification method	N/A	ImageJ open source software [36]	N/A	FFT anisotropy [13]
Electrical conductivity κ [S/m]	$4 \cdot 10^{-3}$ [44] – 0.8 [12]	10^{-9} [26] – $4 \cdot 10^{-3}$ [36]	50 [37]	$4.38 \cdot 10^{-13}$ [7] – 5000 [42]

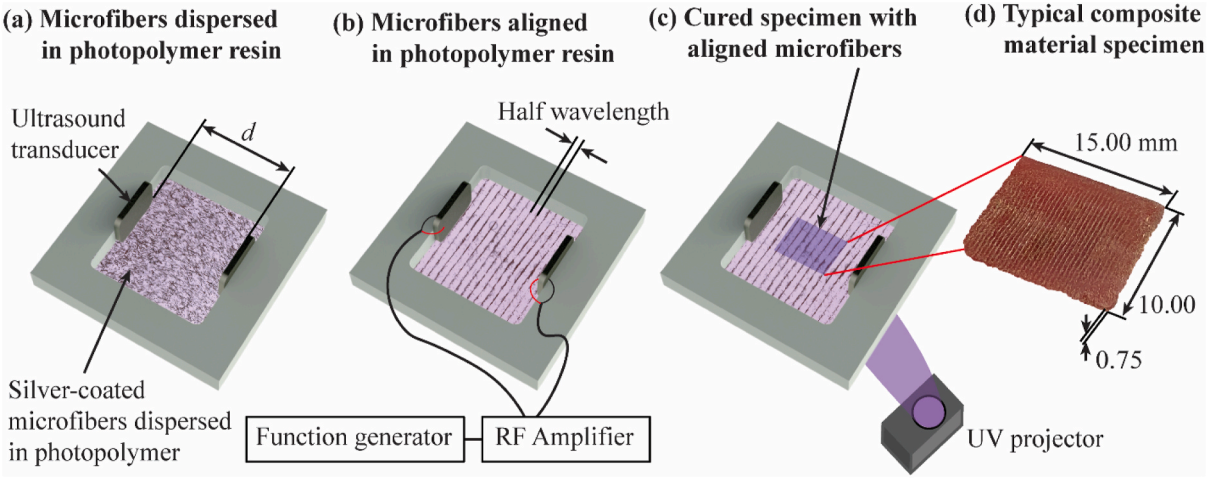

Fig. 1. (a) Schematic of an ultrasound DSA reservoir, with a picture of conductive silver-coated glass microfibers dispersed in photopolymer resin. (b) Picture of microfibers that align at the nodes of a standing ultrasound wave field established between two ultrasound transducers driven by a function generator and RF amplifier. (c) Selective UV exposure initiates photopolymer resin thermosetting and fixates the aligned microfibers in place. (d) Picture of a typical composite material specimen with lines of aligned silver-coated glass microfibers (silver) in photopolymer resin (red) resulting from fabrication process steps (a)–(c). (For interpretation of the references to color in this figure legend, the reader is referred to the Web version of this article.)

Industries Inc. Conduct-O-Fil AG CLAD 12), within a photopolymer matrix (viscosity 250 cP, Makerjuice Standard). Fig. 1 (a) shows an acrylic 30.4 x 30.0 × 6.0 mm reservoir with a mixture of photopolymer resin and electrically conductive microfibers, and a pair of parallel ultrasound transducers (PZT type SM111, center frequency $f_c = 1.5$ MHz) affixed to opposing walls and separated by distance $d = 36\lambda$. Here, $\lambda = c/f$ is the wavelength of the bulk ultrasound wave in the photopolymer resin, $c = 1305$ m/s is the sound propagating velocity in the photopolymer resin, and $f \approx f_c$ is the operating frequency. We use a sonicator (Hielscher UP200Ht, 35.0 W, 5 min) to disperse the microfibers in the liquid photopolymer resin. Fig. 1 (b) illustrates how the microfibers align at the nodes of the standing ultrasound wave field, spaced a half wavelength apart [46,47], after we energize the ultrasound transducers with a function generator (Tektronix AFG 3102) and a radio frequency (RF) amplifier (E&I 2100L). Fig. 1 (c) depicts the SLA process, i.e., selective curing of the photopolymer resin with a UV light source (data projector ViewSonic PJD7822HDL), which fixates the aligned microfibers in place. Finally, Fig. 1 (d) shows a typical 15.00 x 10.00 × 0.75 mm material specimen with lines of aligned silver-coated glass microfibers resulting from the fabrication process illustrated in Fig. 1 (a)–(c).

We fabricate composite material specimens with a weight fraction $1.0 \leq w_f \leq 4.0\%$ of silver-coated microfibers, and with varying level of alignment, to measure the effect of both parameters on the formation of a percolated microfiber network and, thus, the electrical conductivity of the material specimen. This work builds on earlier work by our research group, in which we measured and characterized macro- and microscale alignment of non-conductive carbon microfibers in photopolymer resin [48]. Leveraging the microfiber alignment characterization method of [48], we quantify the microfiber alignment using the alignment probability p_α. This metric describes the likelihood that a cluster of microfibers aligns parallel to the ultrasound transducers and depends on the microfiber weight fraction, ultrasound transducer power, and distance between the transducers [48]. However, the fabrication process does not allow direct control of the alignment probability p_α. Instead, we control the dimensionless ultrasound transducer input power $P = |V|^2 t^2/(\mu\lambda^3 \mathrm{Re}(Z))$, which determines the alignment probability p_α, and depends on the ultrasound DSA process parameters, with V the ultrasound transducer voltage, t the ultrasound exposure time, μ the dynamic viscosity of the photopolymer resin, and Z the ultrasound transducer impedance [48].

We perform a full-factorial experiment based on two independent fabrication process parameters, the dimensionless ultrasound transducer input power P, and the microfiber weight fraction w_f, considering three (for P) and four (for w_f) treatment levels (see Table 2). We identify treatment limits of each independent parameter such that they represent

Table 2
Treatment levels for independent SLA and ultrasound DSA fabrication process parameters.

Independent fabrication process parameter	Treatment level			
	1	2	3	4
Ultrasound transducer input power P [−]	$2.87 \cdot 10^{13}$	$5.11 \cdot 10^{13}$	$1.07 \cdot 10^{14}$	N/A
Microfiber weight fraction w_f [%]	1.0	2.0	3.0	4.0

extreme values of the fabrication process. The microfiber weight fraction limits derive from practical considerations; $w_f < 1.0\%$ does not reliably create a percolated microfiber network, whereas $w_f > 4.0\%$ drastically increases the viscosity of the photopolymer and microfiber mixture and creates mechanical interlocking of the microfibers, which inhibits alignment. We select the treatment limits of P to fabricate material specimens with $0.22 < p_\alpha < 0.80$, which we have empirically identified as the limits of this fabrication process during preliminary experiments with silver-coated glass microfibers, and in our earlier work with carbon microfibers [48].

Based on initial experiments and calculation, we require a minimum of six material specimen replications of each treatment level combination, when considering 80% statistical power and a 95% confidence interval. However, to further ensure the statistical significance of the results, we fabricate 10–20 material specimens of each treatment level combination, which results in a total of 138 material specimens.

2.2. Image acquisition, processing, and microfiber alignment quantification

We sand and polish the top surface of each material specimen with silicon carbide sanding paper (increasingly fine up to 1200 grit) to remove the top layer of photopolymer resin, expose the electrically conductive microfibers, and enable measuring electrical resistance along the line of aligned microfibers. Additionally, the surface preparation ensures a consistent surface finish for optical imaging. We use an optical microscope (Keyence VHX-5000) to image each material specimen with 100x magnification to quantify the microfiber alignment. Imperfections in the fabrication process or non-uniform microfiber dispersion may cause incomplete microfiber alignment. Hence, we image each material specimen covering a 2.47 × 2.47 mm area (based on a convergence study), after we qualitatively observe the best microfiber alignment in each material specimen.

We quantify the alignment probability p_α according to the method documented in Ref. [48], which we briefly summarize as follows. First, we enhance the contrast between the photopolymer resin and microfibers and convert each optical image to a binary image. Then, we employ a two dimensional fast Fourier transform (FFT) to quantify the anisotropy in each binary image [49], such that the FFT anisotropy Φ represents the distribution of individual microfiber alignment angles θ in the image. Normalizing Φ such that its integral from $-\pi/2 \leq \theta \leq \pi/2$ has unit magnitude results in the probability density function of θ, where $\Phi = f(\theta)$. Finally, we compute the microfiber alignment probability p_α as

$$p_\alpha = \int_{-\Delta\theta}^{\Delta\theta} \Phi(\theta) d\theta \tag{1}$$

Here, the alignment probability p_α represents the likelihood that a cluster of microfibers aligns within $\pm\Delta\theta$ of the desired alignment angle θ_s (note that in this paper θ_s is always such that the microfibers align parallel with the ultrasound transducers). We select $\Delta\theta = 10^\circ$ because when considering the results of all the material specimens in this work, it results in a normally distributed dataset of p_α, which is required for parametric multiple regression analysis. Fig. 2 shows a typical microfiber alignment probability measurement, where we convert (a) an optical microscopy image of a material specimen (100x magnification) into (b) a binary image, and (c) calculate p_α according to Eq. (1).

2.3. Measuring electrical resistance and calculating electrical conductivity

We paint conductive silver electrodes (SPI Supplies 05001-AB) directly onto the microfibers, exposed by sanding and polishing, along the edges of each material specimen. Fig. 3 schematically shows a typical electrical resistance measurement between opposing electrodes in the microfiber alignment direction, using a digital multimeter (Mastech MY-65), which corresponds to the "wire resistance" of an electrical conductor. Each electrode covers approximately 2.5 × 15 mm^2 and opposing electrodes are spaced $L = 5$ mm apart. The electrodes contact approximately 35 conductive lines of aligned microfibers, which prevents quantifying how many individual lines form a complete percolated network between the opposing electrodes. Instead, we consider each specimen as an entire percolated microfiber network. The silver coating of the microfibers is the electrically conductive component of the material specimens and, thus, we use the total volume of silver in each material specimen, derived from the microfiber weight fraction w_f, to calculate electrical conductivity. We perform multiple regression analysis between the continuous electrical conductivity κ of the material specimens and the respective treatment levels of the microfiber weight fraction w_f and the measured alignment probability p_α, which is a function of the non-dimensional power P. We confirm that our dataset satisfies all parametric regression analysis assumptions [50] and evaluate the best-fit model according to the root-mean-square error and p values (considering $p \leq 0.05$ to be statistically significant) of logarithmic, exponential, square root, inverse, and polynomial fits.

The electrical conductivity of conductive and semi-conductive materials typically ranges between $4.35 \cdot 10^{-4} < \kappa < 6.29 \cdot 10^{7}$ S/m [51]. Thus, we categorize the material specimens as either electrically

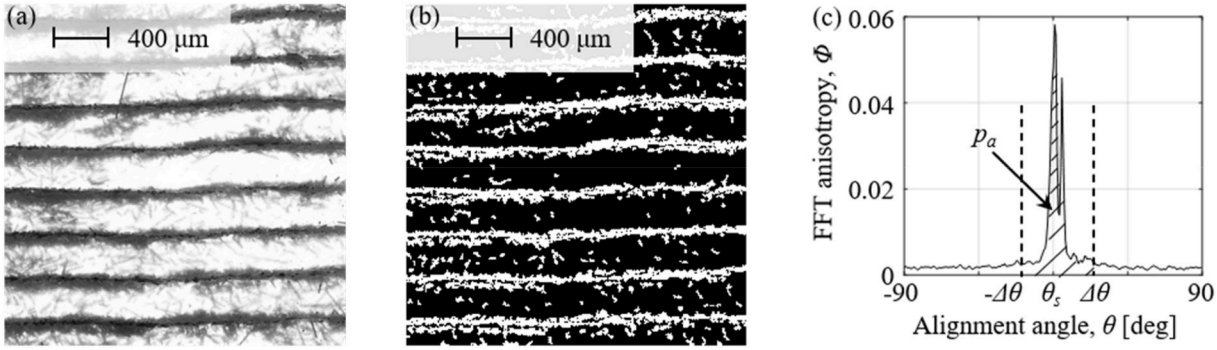

Fig. 2. (a) Grayscale optical microscopy image (100x magnification) of a typical material specimen. (b) Binary conversion of (a). (c) FFT anisotropy of (b), where the hatched area corresponds to the probability that a cluster of microfibers aligns within $\pm\Delta\theta$ of the desired alignment angle θ_s.

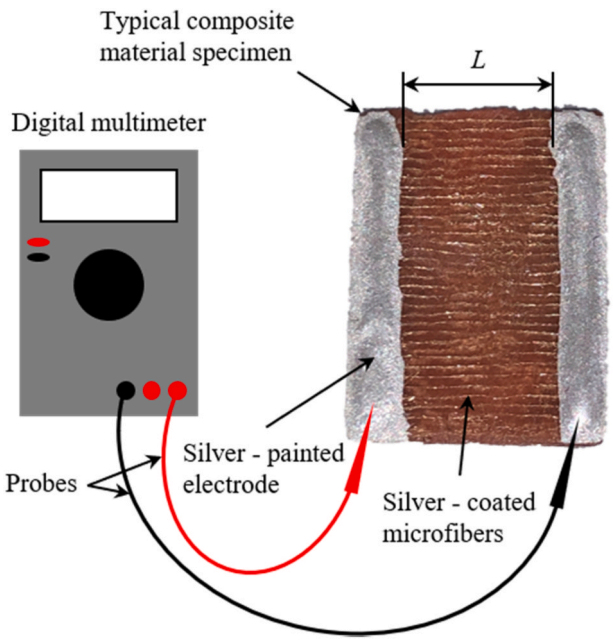

Fig. 3. Typical electrical resistance measurement, using a digital multimeter, between silver-painted electrodes in direct contact with aligned, electrically conductive silver-coated microfibers.

conductive or insulating depending on whether the electrical conductivity is larger or smaller than $4.35 \cdot 10^{-4}$ S/m. We perform logistic regression analysis between the categorical classification of an electrical conductor or insulator of all material specimens and the respective treatment levels of w_f and p_α, thus relating whether a material specimen is electrically conductive or insulating to the fabrication process parameters. Hence, the best-fit logistic regression model predicts whether a material specimen is electrically conductive, according to the model X^2, McFadden R^2, and p values. We confirm that the model complies with logistic regression assumptions [52] and evaluate logarithmic, exponential, square root, inverse, and polynomial fits.

3. Results and discussion

3.1. Electrically conductive versus insulating

Fig. 4 shows an overview of all material specimens in the full-factorial experiment. The rows and columns indicate different treatment levels of the microfiber weight fraction w_f and dimensionless power P, respectively (see Table 2). We list the number of electrically conductive material specimens, classified as electrical conductors or insulators, compared to the total number of specimens of each treatment level combination. We color-code each combination as a function of the fraction of electrically conductive material specimens and include an image of a typical material specimen with lines of aligned conductive microfibers fabricated using each treatment level combination.

A percolated network of electrically conductive microfibers must exist within the insulating polymer matrix material for the material specimen to conduct electricity. Percolation depends on the density of microfibers that agglomerate at the nodes of the standing ultrasound wave field during the ultrasound DSA process, which in turn depends on both the microfiber weight fraction w_f and the alignment probability p_α (controlled by the non-dimensional power P). Fig. 4 shows that the fraction of electrically conductive material specimens increases with increasing microfiber weight fraction w_f and non-dimensional power P. While we did not determine limits of the fabrication process parameters that guarantee electrical conductivity, almost all specimens with $P > 5.11 \cdot 10^{13}$ and $w_f > 3.0$ show a complete percolated network of

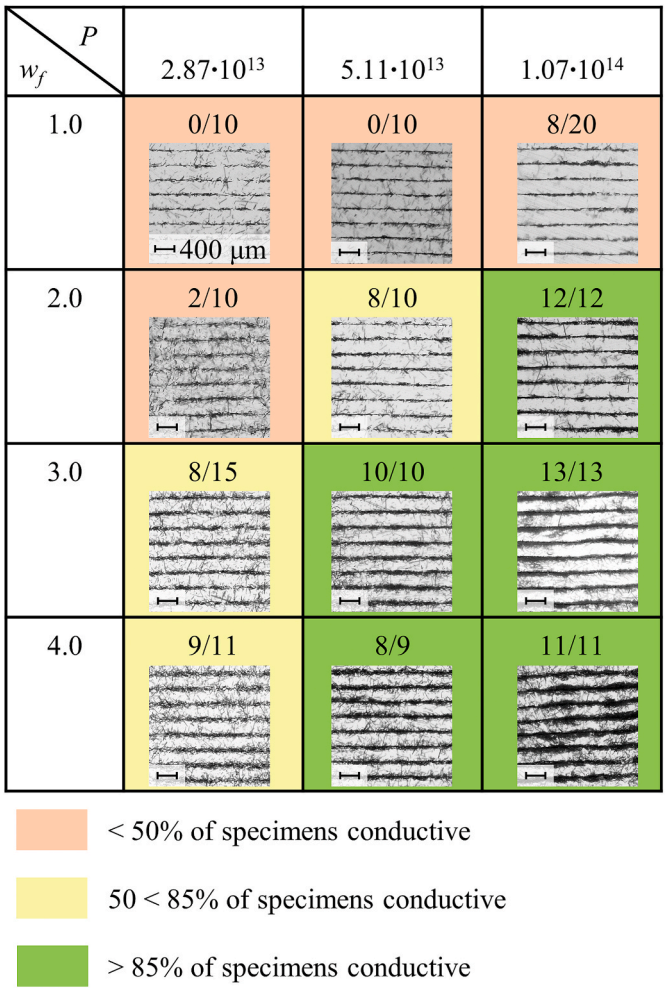

Fig. 4. Overview of all material specimens in the full-factorial experiment, showing the fraction of electrically conductive specimens for each process parameter treatment level combination, including an image of a typical specimen.

conductive microfibers. We also observe that the lines of microfibers show increased alignment with increasing P and increased density with both increasing w_f and P. Physically, increasing P increases the alignment of the microfibers because it increases the amplitude of the ultrasound standing wave and, thus, the corresponding acoustic radiation force that drives the microfibers to the nodes of the standing ultrasound wave field. Additionally, increasing the w_f increases the number of microfibers mixed in the matrix material and, thus, the likelihood that individual microfibers contact each other to form a long-range conductive pathway through the material specimen, independent of their alignment.

Fig. 5 shows optical microscopy images of material specimens fabricated with constant P and different w_f to illustrate the importance of the interaction between P and w_f. We observe from Fig. 5 (a) that even with high P, and therefore well-aligned microfibers, gaps might exist locally between adjacent conductive microfibers when the microfiber weight fraction is low ($w_f = 1.0\%$), preventing a percolated network of microfibers and, thus, electrical conductivity. Additionally, we observe from Fig. 5 (b) that no gaps exist between microfibers when the microfiber weight fraction is high ($w_f = 4.0\%$), even if the alignment of the individual microfibers is imperfect. Note also the substantially thicker lines of aligned microfibers with $w_f = 4.0\%$ compared to $w_f = 1.0\%$, thus locally increasing the microfiber density.

Equation (2) shows the best-fit logistic regression model of the categorical classification of an electrical conductor or insulator of all the

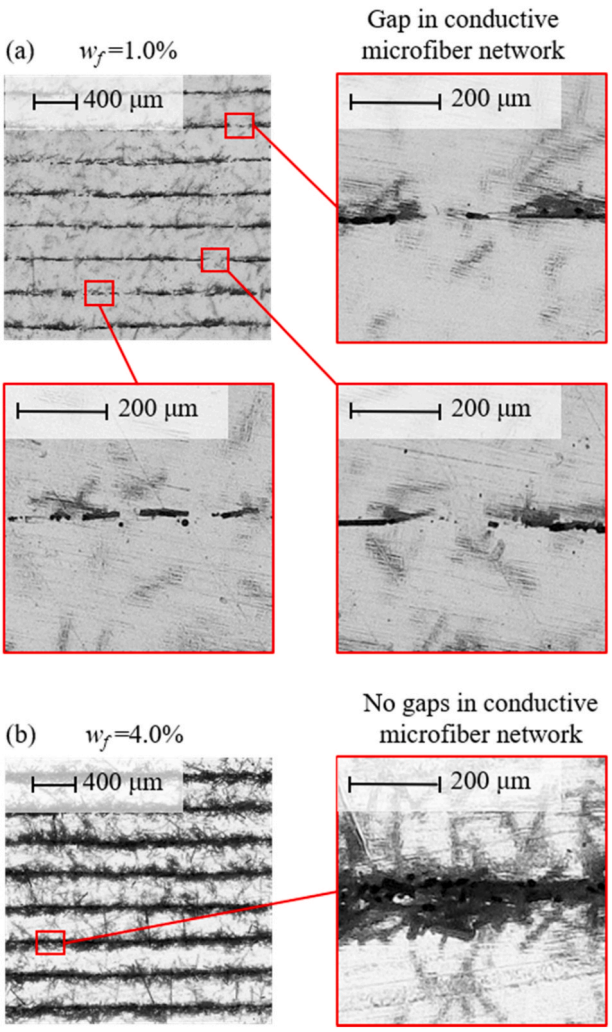

Fig. 5. (a) Electrically insulating material specimen because gaps exist locally between adjacent microfibers due to the low microfiber weight fraction (w_f = 1.0%), despite showing well-aligned electrically conductive microfibers. (b) Electrically conductive material specimen (κ = 153 S/m) because no gaps exist between adjacent microfibers due to high microfiber weight fraction (w_f = 4.0%) and well-aligned electrically conductive microfibers.

material specimens as a function of the microfiber weight fraction w_f and the measured alignment probability p_α, with $X^2 = 88.3$, McFadden $R^2 = 0.50$, and p values of $2.76 \cdot 10^{-9}$ and $6.08 \cdot 10^{-7}$ for w_f and p_α, respectively. In Eq. (2), $p_{conductive} = 1$ when the material specimen is electrically conductive, and $p_{conductive} = 0$ when it is electrically insulating. We note that a McFadden R^2 of 0.2–0.4 is approximately equivalent to an R^2 of 0.7–0.9 for a linear function [53], indicating that the logistic regression model shows an excellent fit of the experimental data.

$$p_{conductive} = \frac{e^{-17.24+2.14w_f+7.60p_\alpha}}{1+e^{-17.24+2.14w_f+7.60p_\alpha}} \quad (2)$$

Fig. 6 shows the probability that a material specimen fabricated with the combined SLA and ultrasound DSA process is electrically conductive $p_{conductive}$, as a function of the alignment probability p_α, for different values of the microfiber weight fraction w_f (identified with different color lines and marker types). The solid lines represent Eq. (2) for different values of w_f, whereas the markers indicate the individual experimental data points, discretely categorized as electrically conductive ($p_{conductive} = 1$) or insulating ($p_{conductive} = 0$) and, thus, not considering continuous values of the electrical conductivity.

Fig. 6 shows that the probability that a material specimen with lines of aligned conductive microfibers is electrically conductive, increases with increasing microfiber alignment probability p_α and weight fraction w_f, respectively. The experimental data matches this trend, illustrated by the different markers at $p_{conductive} = 1$ and $p_{conductive} = 0$, respectively. From Fig. 6 we also observe that specimens with $w_f = 1.0\%$ or $w_f = 4.0\%$ show higher deviation between theoretical and experimental $p_{conductive}$ values than specimens with $w_f = 2.0\%$ and $w_f = 3.0\%$ because they are heavily skewed towards $p_{conductive} = 0$ and $p_{conductive} = 1$, respectively.

We further illustrate the results of Fig. 6 by showing physical data from the material specimens in Fig. 7 (increasing the microfiber weight fraction w_f) and Fig. 8 (increasing the microfiber alignment probability p_α). Figs. 7 and 8 (a)–(c) show schematic representations of the electrically conductive microfibers in the matrix material with increasing alignment probability p_α and microfiber weight fraction w_f, respectively, whereas Figs. 7 and 8 (d)–(i) show optical images with different magnification that illustrate the effects of p_α and w_f on the formation of a percolated microfiber network.

Fig. 7 (a)–(c) illustrate that increasing w_f creates increasingly closely packed individual microfibers (black), which are more likely to make contact to form a percolated network of electrically conductive microfibers (red). Fig. 7 (d)–(f) show that the density of a single line of aligned microfibers increases with increasing w_f, again increasing the likelihood that electrically conductive microfibers make contact and form a percolated network. Similarly, Fig. 7 (g)–(i) show multiple lines of aligned microfibers. We observe that the thickness of these lines of aligned microfibers increases with increasing w_f because more microfibers agglomerate at the nodes of the standing ultrasound wave. This again increases contact between microfibers and the likelihood of forming a percolated network. Fig. 8 (a)–(c) illustrate that increasing the alignment probability p_α increases the likelihood that individual microfibers (black) make contact (red) and form a percolated network. Fig. 8 (d)–(f) show that the density of a single line of aligned microfibers increases with increasing p_α, again increasing the likelihood that electrically conductive microfibers make contact and form a percolated network. Similarly, Fig. 8 (g)–(i) show multiple lines of aligned microfibers. We observe that the density of these lines of aligned microfibers increases with increasing p_α because increased alignment of the microfibers exists at the nodes of the standing ultrasound wave. This again increases contact between microfibers and the likelihood of forming a percolated network.

3.2. Continuous electrical conductivity

Fig. 9 shows the electrical conductivity κ of the electrically conductive material specimens from the full-factorial experiment as a function of the measured microfiber alignment probability p_α. Marker types and colors indicate different microfiber weight fractions w_f.

From Fig. 9 we observe that p_α increases and then decreases with increasing w_f, for $w_f \geq 1.0$ and $w_f \geq 2.0$, respectively. This suggests that the nodes of the ultrasound wave field saturate with microfibers when $1.0 \leq w_f \leq 2.0$, causing microfibers to entangle and preventing additional microfibers from aligning at the nodes. The electrical conductivity κ of the conductive material specimens varies from 31 to 793 S/m, but statistical analysis does not reveal significant trends within the dataset of electrically conductive material specimens as a function of fabrication process parameters. This means that although p_α and w_f are critical in predicting whether a material specimen will be electrically conductive (see Eq. (2)), these process parameters do not significantly affect the magnitude of the electrical conductivity of a material specimen within an existing percolated network of electrically conductive fibers. Once an electrically conductive pathway exists, electrical current can flow independent of the shape (alignment) or geometry (density) of that pathway.

Although no publications in the open literature characterize the electrical conductivity of polymer matrix composite materials with aligned microfibers as a function of the microfiber weight fraction w_f

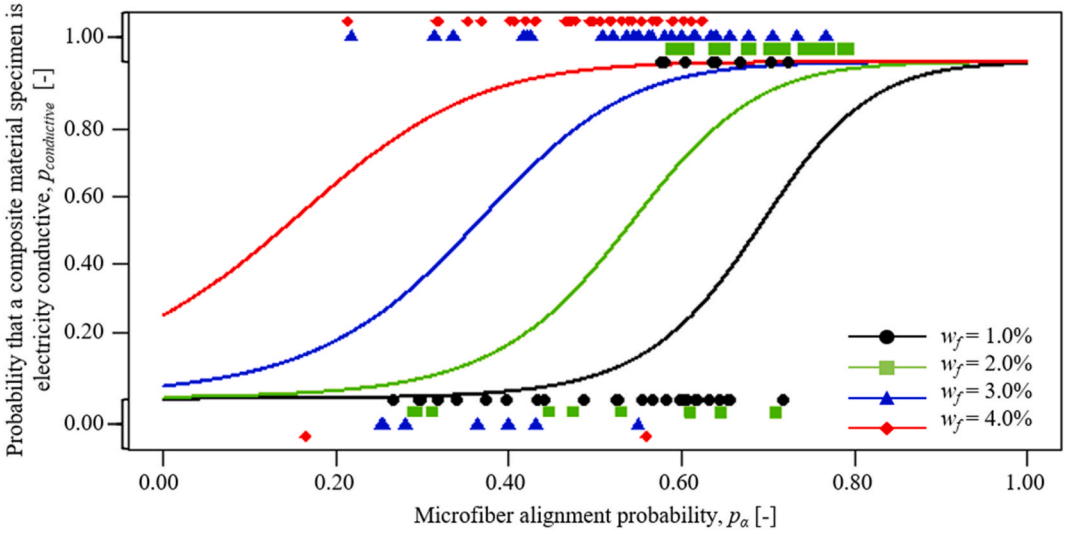

Fig. 6. Probability that a material specimen is electrically conductive $p_{conductive}$ as a function of microfiber alignment probability p_α and weight fraction w_f, also showing each individual experimental datapoint.

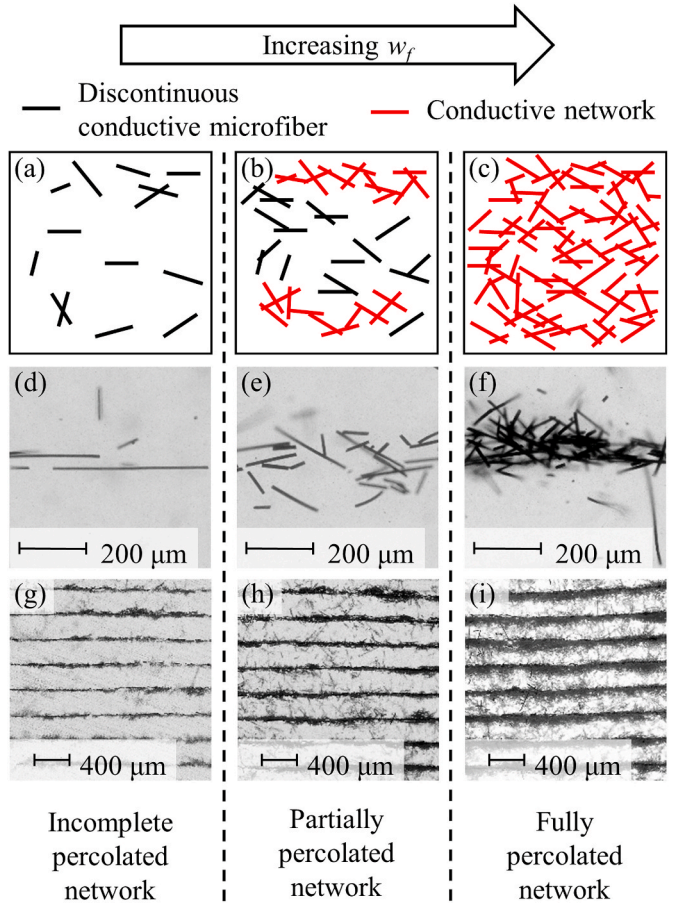

Fig. 7. (a)–(c) Schematic illustrating that a percolated network of discontinuous conductive microfibers forms with increasing microfiber weight fraction w_f. (d)–(f) Optical images of individual microfibers, from a line of aligned microfibers, illustrating that increasing w_f causes microfibers to make contact and form a percolated network. (g)–(i) Optical images of sections of material specimens with multiple lines of aligned microfibers, illustrating that increasing w_f causes a higher microfiber density at the nodes of the standing ultrasound wave, which promotes the formation of a percolated network of electrically conductive microfibers.

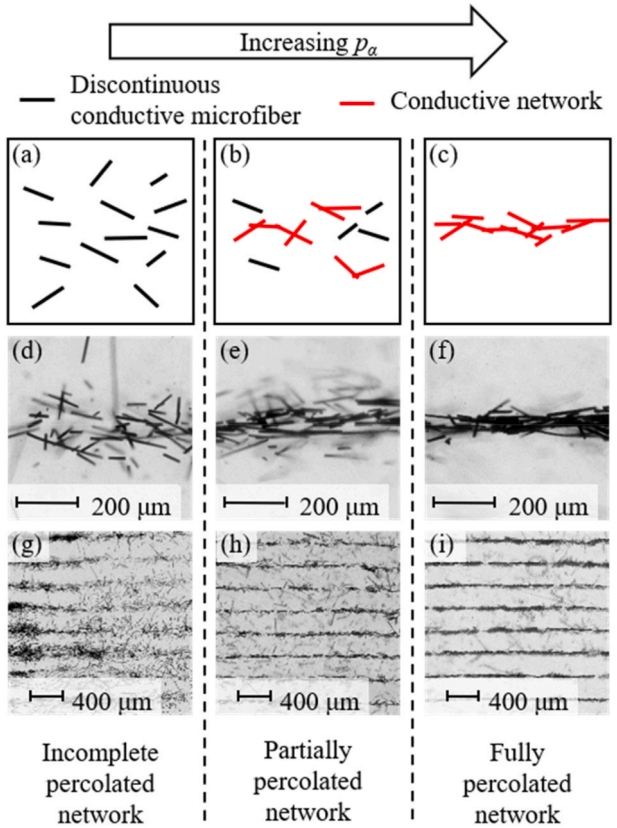

Fig. 8. (a)–(c) Schematic illustrating that a percolated network of electrically conductive microfibers forms with increasing alignment probability p_α. (d)–(f) Optical images of individual microfibers, from a line of aligned microfibers, illustrating that increasing p_α causes microfibers to make contact and form a percolated network. (g)–(i) Optical images of sections of material specimens with multiple lines of aligned microfibers and constant w_f, showing that increasing p_α increases the microfiber density at the nodes of the standing ultrasound wave, which promotes the formation of a percolated network of electrically conductive microfibers.

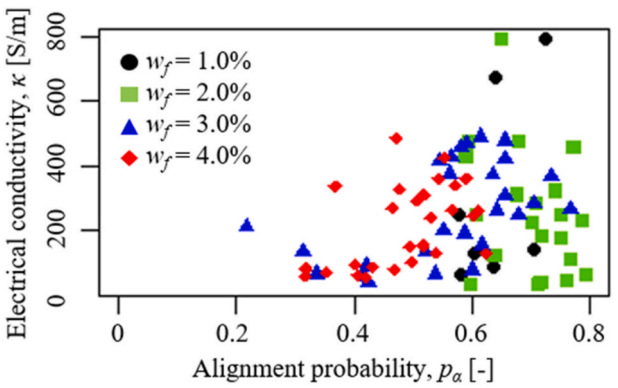

Fig. 9. Electrical conductivity κ as a function of microfiber alignment probability p_α, for different values of the microfiber weight fraction w_f.

and alignment probability p_α, several groups have published related studies. Our findings agree with the results documented by Melchert et al., who fabricated flexible polymer matrix composite materials with silver-coated glass and uncoated carbon microfibers aligned using ultrasound DSA [42]. They reported a maximum electrical conductivity of $\kappa = 5000$ and 10 S/m, for silver-coated glass and uncoated carbon microfibers, respectively, and found that the magnitude of κ remained almost constant, independent of w_f. Oliva-Avilés et al. fabricated polymer matrix composite materials with aligned MWCNTs using an electric field, and reported that the electrical conductivity κ increased with increasing microfiber weight fraction for $0.1 \leq w_f \leq 0.5\%$ with a maximum conductivity κ of approximately 0.05 S/m (for $w_f = 0.5\%$) [25], which is four orders of magnitude lower than the material specimens we have fabricated for this paper. We speculate that this difference is because the silver-coated microfibers are more electrically conductive than the uncoated MWCNTs. Similarly, Ma et al. aligned nickel-infused CNTs in an epoxy matrix using a magnetic field, and measured that the electrical conductivity κ increased with increasing weight fraction for $0.5 < w_f < 5.0\%$ with maximum κ of $4 \cdot 10^{-3}$ S/m [36], which is inconsistent with our findings. Postiglione et al. printed electrically conductive PLA composite materials with aligned MWCNTs and also measured that electrical the conductivity κ increased with increasing MWCNT weight fraction, for $0.5 < w_f < 10.0\%$, up to approximately 50 S/m [37], which is on the same order of magnitude as composite materials we fabricated for this paper. Finally, Ladani et al. fabricated epoxy composite materials with carbon nanofibers (CNFs) or graphene nanoplatelets (GNPs) aligned using an electric field and also measured that the electrical conductivity κ increased with increasing filler weight fraction w_f, up to approximately 0.01 S/m and 10^{-6} S/m, for CNFs and GNPs, respectively [5]. Furthermore, it is evident that electrical conductivity depends on the filler material properties, which explains differences between our work and that of other groups.

Characterizing the probability that a composite material is electrically conductive as a function of the fabrication process parameters, including the microfiber weight fraction w_f and alignment probability p_α, is an important step towards using ultrasound DSA as a fabrication process for engineered polymer matrix composite materials with designer electrical properties. For instance, by leveraging the regression model in this paper, we can estimate the minimum microfiber weight fraction w_f and microfiber alignment probability p_α required to fabricate an electrically conductive material specimen. Such materials are of interest to a myriad of engineering applications, including flexible electronics, chemical or biological sensors, and stretchable strain sensors, amongst others. Furthermore, this paper shows that the combined SLA and ultrasound DSA method enables the fabrication of macroscale material specimens, thus demonstrating the dimensional scalability of the technique. Limitations of the dimensional scalability include input power to the ultrasound transducers, as this might locally heat the photopolymer resin and cause boiling, and photopolymer viscosity, which affects ultrasound wave attenuation and the magnitude of viscous drag forces acting on the filler material. Additionally, increasing the weight fraction of the filler material increases the viscosity of the photopolymer/filler material mixture and may change the curing characteristics of the photopolymer.

We also emphasize that ultrasound DSA functions independent of the material properties of the filler material and, thus, while we use silver-coated microfibers for this study, one could use the fabrication process with any other type of filler material and repeat the study to evaluate electrical conductivity. While the results might change, the method and approach documented in this paper remain valid, independent of the specific material combination.

4. Conclusions

A percolated network of electrically conductive microfibers is required to obtain long-range electrical conductivity throughout an engineered polymer matrix composite material. Percolation is driven by the density of microfibers along the conductive path. Ultrasound DSA aligns microfibers at the nodes of a standing ultrasound wave and the microfiber weight fraction determines the number of microfibers that agglomerates at the nodes of the standing ultrasound wave. Thus, the density of microfibers along the conductive path depends on both microfiber alignment and microfiber weight fraction. Specifically:

1. The percolation threshold decreases with increasing microfiber alignment probability because microfiber density at the nodes of the standing ultrasound wave increases with increasing alignment probability, which increases contact between neighboring microfibers.
2. The alignment probability required for electrical conductivity decreases with increasing microfiber weight fraction because adding more microfibers to a composite material specimen increases microfiber density and, therefore, increases contact between neighboring microfibers, independent of alignment probability.

These results agree with results documented by others using different fabrication methods, as highlighted in the introduction and discussion of this paper. However, we emphasize that the combined ultrasound DSA and SLA fabrication process offers flexibility in terms of specimen geometry through the SLA process, spatial arrangement and alignment of the discontinuous filler material through the ultrasound DSA process, and dimensional scalability through the combination of both.

We also conclude that although microfiber weight fraction and alignment probability are crucial in predicting if a composite material specimen will be electrically conductive, the fabrication process parameters do not significantly affect the magnitude of electrical conductivity of a material specimen with an existing percolated network. Understanding the relationship between the ultrasound DSA process parameters and the resulting electrical conductivity of a composite material specimen is an important step towards fabricating macroscale engineered polymer matrix composite materials with embedded percolated networks of aligned and electrically conductive microfibers for use in a myriad of engineering applications.

Author statement

KN and BR designed the experiments, KN performed the experiments, KN and BR analyzed the data and wrote the manuscript.

Declaration of competing interest

The authors declare that they have no known competing financial interests or personal relationships that could have appeared to influence the work reported in this paper.

Acknowledgments

This research was supported by the Army Research Office under contract no. W911NF-16-1-0457.

References

[1] Park S-J, Seo M-K. Chapter 7 - types of composites. Interface Sci. Technol. 2011: 501–629.
[2] Kabir SMF, Mathur K, Seyam AFM. A critical review on 3D printed continuous fiber-reinforced composites: history, mechanism, materials and properties. Compos Struct 2020;232:111476. https://doi.org/10.1016/j.compstruct.2019.111476.
[3] Sugama T, Gawlik K. Milled carbon microfiber-reinforced poly(phenylenesulfide) coatings for abating corrosion of carbon steel. Polym Polym Compos 2003;11: 161–9. https://doi.org/10.1177/096739110301100301.
[4] Thankappan A, Thomas S, Nampoori VPN. Novel composites based on polymer micro-rods for photonic device applications. Opt Laser Technol 2014;58:63–70. https://doi.org/10.1016/j.optlastec.2013.10.017.
[5] Ladani RB, Wu S, Kinloch AJ, Ghorbani K, Zhang J, Mouritz AP, et al. Multifunctional properties of epoxy nanocomposites reinforced by aligned nanoscale carbon. Mater Des 2016;94:554–64. https://doi.org/10.1016/j.matdes.2016.01.052.
[6] Singh NP, Gupta VK, Singh AP. Graphene and carbon nanotube reinforced epoxy nanocomposites: a review. Polymer (Guildf) 2019;180:121724. https://doi.org/10.1016/j.polymer.2019.121724.
[7] Yunus DE, Sohrabi S, He R, Shi W, Liu Y. Acoustic patterning for 3D embedded electrically conductive wire in stereolithography. J Micromech Microeng 2017;27. https://doi.org/10.1088/1361-6439/aa62b7.
[8] Herren B, Larson P, Saha M, Liu Y. Enhanced electrical conductivity of carbon nanotube-based elastomer nanocomposites prepared by microwave curing. Polymers (Basel) 2019;11:1212. https://doi.org/10.3390/polym11071212.
[9] Goh PS, Ismail AF, Ng BC. Directional alignment of carbon nanotubes in polymer matrices: contemporary approaches and future advances. Compos Part A Appl Sci Manuf 2014;56:103–26. https://doi.org/10.1016/j.compositesa.2013.10.001.
[10] Lu L, Zhang Z, Xu J, Pan Y. 3D-printed polymer composites with acoustically assembled multidimensional filler networks for accelerated heat dissipation. Compos B Eng 2019;174. https://doi.org/10.1016/j.compositesb.2019.106991.
[11] Greenhall J, Homel LJ, Raeymaekers B. Ultrasound directed self-assembly processing of nanocomposites with ultra-high carbon nanotube weight fractions. J Compos Mater 2018;53. https://doi.org/10.1177/0021998318801452.
[12] Gupta P, Rajput M, Singla N, Kumar V, Lahiri D. Electric field and current assisted alignment of CNT inside polymer matrix and its effects on electrical and mechanical properties. Polym (United Kingdom) 2016;89:119–27. https://doi.org/10.1016/j.polymer.2016.02.025.
[13] Greenhall J, Raeymaekers B. 3D printing macroscale engineered materials using ultrasound directed self-assembly and stereolithography. Adv Mater Technol 2017; 2. https://doi.org/10.1002/admt.201700122.
[14] Park S, Vosguerichian M, Bao Z. A review of fabrication and applications of carbon nanotube film-based flexible electronics. Nanoscale 2013;5:1727–52. https://doi.org/10.1039/c3nr33560g.
[15] Cheung W, Chiu PL, Parajuli RR, Ma Y, Ali SR, He H. Fabrication of high performance conducting polymer nanocomposites for biosensors and flexible electronics: summary of the multiple roles of DNA dispersed and functionalized single walled carbon nanotubes. J Mater Chem 2009;19:6465–80. https://doi.org/10.1039/b823065j.
[16] Kang I, Schulz MJ, Kim JH, Shanov V, Shi D. A carbon nanotube strain sensor for structural health monitoring. Smart Mater Struct 2006;15:737–48. https://doi.org/10.1088/0964-1726/15/3/009.
[17] Lee JH, Jang YK, Hong CE, Kim NH, Li P, Lee HK. Effect of carbon fillers on properties of polymer composite bipolar plates of fuel cells. J Power Sources 2009; 193:523–9. https://doi.org/10.1016/j.jpowsour.2009.04.029.
[18] Socher R, Krause B, Hermasch S, Wursche R, Pötschke P. Electrical and thermal properties of polyamide 12 composites with hybrid fillers systems of multiwalled carbon nanotubes and carbon black. Compos Sci Technol 2011;71:1053–9. https://doi.org/10.1016/j.compscitech.2011.03.004.
[19] Bai JB, Allaoui A. Effect of the length and the aggregate size of MWNTs on the improvement efficiency of the mechanical and electrical properties of nanocomposites - experimental investigation. Compos Part A Appl Sci Manuf 2003; 34:689–94. https://doi.org/10.1016/S1359-835X(03)00140-4.
[20] Monti M, Rallini M, Puglia D, Peponi L, Torre L, Kenny JM. Morphology and electrical properties of graphene-epoxy nanocomposites obtained by different solvent assisted processing methods. Compos Part A Appl Sci Manuf 2013;46: 166–72. https://doi.org/10.1016/j.compositesa.2012.11.005.
[21] Chandrasekaran S, Seidel C, Schulte K. Preparation and characterization of graphite nano-platelet (GNP)/epoxy nano-composite: mechanical, electrical and thermal properties. Eur Polym J 2013;49:3878–88. https://doi.org/10.1016/j.eurpolymj.2013.10.008.
[22] Wu S, Ladani RB, Ravindran AR, Zhang J, Mouritz AP, Kinloch AJ, et al. Aligning carbon nanofibres in glass-fibre/epoxy composites to improve interlaminar toughness and crack-detection capability. Compos Sci Technol 2017;152:46–56. https://doi.org/10.1016/j.compscitech.2017.09.007.
[23] Bauhofer W, Kovacs JZ. A review and analysis of electrical percolation in carbon nanotube polymer composites. Compos Sci Technol 2009;69:1486–98. https://doi.org/10.1016/j.compscitech.2008.06.018.
[24] Du F, Fischer JE, Winey KI. Effect of nanotube alignment on percolation conductivity in carbon nanotube/polymer composites. Phys Rev B Condens Matter 2005;72:1–4. https://doi.org/10.1103/PhysRevB.72.121404.
[25] Oliva-Avilés AI, Avilés F, Sosa V, Oliva AI, Gamboa F. Dynamics of carbon nanotube alignment by electric fields. Nanotechnology 2012;23. https://doi.org/10.1088/0957-4484/23/46/465710.
[26] Wu S, Zhang J, Ladani RB, Ghorbani K, Mouritz AP, Kinloch AJ, et al. A novel route for tethering graphene with iron oxide and its magnetic field alignment in polymer nanocomposites. Polymer (Guildf) 2016;97:273–84. https://doi.org/10.1016/j.polymer.2016.05.024.
[27] Niendorf K, Raeymaekers B. Additive manufacturing of polymer matrix composite materials with aligned or organized filler Material : a review. Adv Eng Mater 2021: 1–18. https://doi.org/10.1002/adem.202001002. 2001002.
[28] Delmonte J. Molding and casting of metal/polymer composites. Boston, MA: Met. Compos. Springer US; 1990. https://doi.org/10.1007/978-1-4684-1446-2_3.
[29] Gibson I, Rosen D, Stucker B. Additive manufacturing technologies: 3D printing, rapid prototyping, and direct digital manufacturing. second ed. Springer US; 2015.
[30] Yang Y, Chen Z, Song X, Zhang Z, Zhang J, Shung KK, et al. Biomimetic anisotropic reinforcement architectures by electrically assisted nanocomposite 3D printing. Adv Mater 2017;29:1–8. https://doi.org/10.1002/adma.201605750.
[31] Sharma A, Tripathi B, Vijay YK. Dramatic Improvement in properties of magnetically aligned CNT/polymer nanocomposites. J Membr Sci 2010;361: 89–95. https://doi.org/10.1016/j.memsci.2010.06.005.
[32] Moaseri E, Fotouhi M, Bazubandi B, Karimi M, Baniadam M, Maghrebi M. Two-dimensional reinforcement of epoxy composites: alignment of multi-walled carbon nanotubes in two directions. Adv Compos Mater 2020;29:547–57. https://doi.org/10.1080/09243046.2020.1718361.
[33] Kamat PV, Thomas KG, Barazzouk S, Girishkumar G, Vinodgopal K, Meisel D. Self-assembled linear bundles of single wall carbon nanotubes and their alignment and deposition as a film in a dc field. J Am Chem Soc 2004;126:10757–62. https://doi.org/10.1021/ja0479888.
[34] Tanimoto Y, Fujiwara M, Shimomura Y, Mukouda I, Oki E, Hamada M. Magnetic orientation and magnetic properties of a single carbon nanotube. J Phys Chem A 2002;105:4383–6. https://doi.org/10.1021/jp004620y.
[35] Khan SU, Pothnis JR, Kim JK. Effects of carbon nanotube alignment on electrical and mechanical properties of epoxy nanocomposites. Compos Part A Appl Sci Manuf 2013;49:26–34. https://doi.org/10.1016/j.compositesa.2013.01.015.
[36] Ma C, Liu HY, Du X, Mach L, Xu F, Mai YW. Fracture resistance, thermal and electrical properties of epoxy composites containing aligned carbon nanotubes by low magnetic field. Compos Sci Technol 2015;114:126–35. https://doi.org/10.1016/j.compscitech.2015.04.007.
[37] Postiglione G, Natale G, Griffini G, Levi M, Turri S. Conductive 3D microstructures by direct 3D printing of polymer/carbon nanotube nanocomposites via liquid deposition modeling. Compos Part A Appl Sci Manuf 2015;76:110–4. https://doi.org/10.1016/j.compositesa.2015.05.014.
[38] Prisbrey M, Greenhall J, Guevara Vasquez F, Raeymaekers B. Ultrasound directed self-assembly of three-dimensional user-specified patterns of particles in a fluid medium. J Appl Phys 2017;121. https://doi.org/10.1063/1.4973190.
[39] Prisbrey M, Raeymaekers B. Aligning high-aspect-ratio particles in user-specified orientations with ultrasound-directed self-assembly. Phys Rev Appl 2019;12: 014014. https://doi.org/10.1103/PhysRevApplied.12.014014.
[40] Collino RR, Ray TR, Fleming RC, Sasaki CH, Haj-Hariri H, Begley MR. Acoustic field controlled patterning and assembly of anisotropic particles. Extrem Mech Lett 2015;5:37–46. https://doi.org/10.1016/j.eml.2015.09.003.
[41] Kinsler LE, Frey AR, Coppens AB, Sanders JV. Fundamentals of acoustics. New York: John Wiley; 2000.
[42] Melchert DS, Collino RR, Ray TR, Dolinski N, Friedrich L, Begley MR, et al. Flexible conductive composites with programmed electrical anisotropy using acoustophoresis. Adv Mater Technol 2019:1–8. https://doi.org/10.1002/admt.201900586.
[43] Ladani RB, Wu S, Kinloch AJ, Ghorbani K, Zhang J, Mouritz AP, et al. Improving the toughness and electrical conductivity of epoxy nanocomposites by using aligned carbon nanofibres. Compos Sci Technol 2015;117:146–58. https://doi.org/10.1016/j.compscitech.2015.06.006.
[44] Choi ES, Brooks JS, Eaton DL, Al-Haik MS, Hussaini MY, Garmestani H, et al. Enhancement of thermal and electrical properties of carbon nanotube polymer composites by magnetic field processing. J Appl Phys 2003;94:6034–9. https://doi.org/10.1063/1.1616638.
[45] Wadsworth P, Nelson I, Porter DL, Raeymaekers B, Naleway SE. Manufacturing bioinspired flexible materials using ultrasound directed self-assembly and 3D printing. Mater Des 2020:185. https://doi.org/10.1016/j.matdes.2019.108243.
[46] Greenhall J, Guevara Vasquez F, Raeymaekers B. Continuous and unconstrained manipulation of micro-particles using phase-control of bulk acoustic waves. Appl Phys Lett 2013;103. https://doi.org/10.1063/1.4819031.
[47] King LV. On the acoustic radiation pressure on spheres. Proc R Soc A Math Phys Eng Sci 1934;147:212–40. https://doi.org/10.1098/rspa.1934.0215.
[48] Niendorf K, Raeymaekers B. Quantifying macro- and microscale alignment of carbon microfibers in polymer-matrix composite materials fabricated using ultrasound directed self-assembly and 3D-printing. Compos Part A Appl Sci Manuf 2020;129:105713. https://doi.org/10.1016/j.compositesa.2019.105713.
[49] Ayres CE, Jha BS, Meredith H, Bowman JR, Bowlin GL, Henderson SC, et al. Measuring fiber alignment in electrospun scaffolds : a user ' s guide to the 2D fast Fourier transform approach. J Biomater Sci Polym Ed 2008;19:603–21.
[50] Sen A, Srivastava M. Regression analysis: theory, methods and applications. New York: Springer-Verlag; 1990.

[51] Ling SJ, Sanny J, Moebs W, Friedman G, Druger SD, Kolakowska A, et al. University physicsvol. 2. Houston, Texas: OpenStax; 2016.
[52] Hosmer DW, Lemeshow S, Sturdivant RX. Applied logistic regression. third edition. third ed. Hoboken, NJ: John Wiley and Sons; 2013.
[53] Louviere J, Hensher D, Swait J, Adamowicz W. Stated choice methods: analysis and applications. New York: Cambridge University Press; 2000. https://doi.org/10.1017/CBO9780511753831.